



Kent Academic Repository

Chitty, Claudia, Kuliga, Kinga and Xue, Wei-Feng (2024) *Atomic force microscopy 3D structural reconstruction of individual particles in the study of amyloid protein assemblies*. *Biochemical Society Transactions*, 52 (2). pp. 761-771. ISSN 0300-5127.

Downloaded from

<https://kar.kent.ac.uk/105896/> The University of Kent's Academic Repository KAR

The version of record is available from

<https://doi.org/10.1042/BST20230857>

This document version

Author's Accepted Manuscript

DOI for this version

<https://doi.org/10.22024/UniKent/01.02.105896.3429838>

Licence for this version

CC BY (Attribution)

Additional information

For the purpose of open access, the author has applied a CC BY public copyright licence to any Author Accepted Manuscript version arising from this submission.

Versions of research works

Versions of Record

If this version is the version of record, it is the same as the published version available on the publisher's web site. Cite as the published version.

Author Accepted Manuscripts

If this document is identified as the Author Accepted Manuscript it is the version after peer review but before type setting, copy editing or publisher branding. Cite as Surname, Initial. (Year) 'Title of article'. To be published in ***Title of Journal***, Volume and issue numbers [peer-reviewed accepted version]. Available at: DOI or URL (Accessed: date).

Enquiries

If you have questions about this document contact ResearchSupport@kent.ac.uk. Please include the URL of the record in KAR. If you believe that your, or a third party's rights have been compromised through this document please see our [Take Down policy](https://www.kent.ac.uk/guides/kar-the-kent-academic-repository#policies) (available from <https://www.kent.ac.uk/guides/kar-the-kent-academic-repository#policies>).

1
2
3
4
5
6
7
8
9
10
11
12
13
14
15
16
17
18
19
20
21
22
23

Atomic force microscopy 3D structural reconstruction of individual particles in the study of amyloid protein assemblies

Claudia Chitty, Kinga Kuliga, Wei-Feng Xue*

School of Biosciences, Division of Natural Sciences, University of Kent, CT2 7NJ, Canterbury, UK;

* Correspondence to W.F.Xue@kent.ac.uk

Key words: atomic force microscopy / structural biology / amyloid / helix / filaments / image analysis

24

25 **Abstract**

26

27 Recent developments in Atomic Force Microscopy (AFM) image analysis have made 3D
28 structural reconstruction of individual particles observed on 2D AFM height images a reality.
29 Here, we review the emerging contact point reconstruction AFM (CPR-AFM) methodology
30 and its application in 3D reconstruction of individual helical amyloid filaments in the context
31 of the challenges presented by the structural analysis of highly polymorphous and
32 heterogeneous amyloid protein structures. How individual particle level structural analysis
33 can contribute to resolving the amyloid polymorph structure-function relationships, the
34 environmental triggers leading to protein misfolding and aggregation into amyloid species,
35 the influences by the conditions or minor fluctuations in the initial monomeric protein
36 structure on the speed of amyloid fibril formation, and the extent of the different types of
37 amyloid species that can be formed, are discussed. Future perspectives in the capabilities of
38 AFM based 3D structural reconstruction methodology exploiting synergies with other recent
39 AFM technology advances are also discussed to highlight the potential of AFM as an
40 emergent general, accessible and multimodal structural biology tool for the analysis of
41 individual bio-molecules.

42

43

44

45

46 **Introduction**

47

48 Since the development of atomic force microscopy (AFM) in the mid-1980s ¹, there have
49 been many notable advances in the capabilities of AFM. Developments leveraging AFM's
50 sensitivity to force in the pico-Newton range well below the rupture force of single chemical
51 bonds, high signal-to-ratio three-dimensional (3D) multimodal imaging, and capabilities for
52 studying soft materials and biological systems under ambient conditions in air or in fluid
53 chambers have together enabled imaging of biomolecules to high details ². AFM is now
54 emerging as an indispensable tool for the structural analysis of single, individual helical
55 amyloid filament structures ^{3,4}.

56

57 Amyloid structures represent a class of filamentous, proteinaceous assemblies typically 5-20
58 nm in width and between few nanometres to several micrometres in length ⁵⁻⁸. All amyloid
59 fibrils share a common core structural feature, the cross- β arrangement where β -sheets run
60 perpendicularly to the fibril axis ⁹⁻¹¹. However, variations in the precise packing
61 arrangements of the β -sheets result in multiple fibril structures, often referred to as
62 polymorphs, that can form from the same peptide or protein building blocks even under
63 identical conditions ^{12,13}. The individual polymorph structures of amyloid fibrils may underlie
64 the different biological responses amyloid elicit and the varied associations of different fibril
65 polymorphs with different neurodegenerative diseases ^{6,14}. To resolve the extent of amyloid
66 polymorphism, to understand the structure-function relationships of these complex
67 biomolecular assemblies and to develop effective therapeutics targeting specific polymorph
68 structures, one must be able to map the population of amyloid structures in complex mixtures
69 using a technique that can interrogate individual or rarely populated structures in addition to

70 those in the majority. Recent advances in AFM image analysis have made such endeavour
71 possible where 3D structural reconstruction can be carried out from just one individual
72 filament observed without the need to average across particles using AFM height topology
73 images¹⁵⁻¹⁷.

74

75 A range of current AFM analysis software tools and workflows for extracting structural
76 information from single biomolecules, for example Gwyddion¹⁸, FibreApp¹⁹,
77 BioAFMviewer²⁰, TopoStats²¹ and NanoLocz²², are based on detailed 2D analysis of AFM
78 height topology images. Here, we review the recent advances in 3D structural analysis of
79 individual helical amyloid filaments with contact point reconstruction AFM (CPR-AFM)^{4,17}.
80 We discuss the links and the synergies to existing analysis workflows, and the exciting future
81 outlooks for AFM as a powerful and unique emergent technology capable of resolving the
82 structure and dynamics of bio-molecules, one individual particle at time.

83

84

85 **Challenges in the structural analysis of polymorphic amyloid assemblies**

86

87 Amyloid fibrils are associated with disorders including Alzheimer's disease (AD),
88 Parkinson's disease (PD), type II diabetes and various systemic amyloidosis where the
89 accumulation and deposition of amyloid fibrils occur in affected tissues and organs^{6,8}. In
90 some instances, amyloid assemblies can also play crucial roles in providing regular
91 physiological functions in a broad range of hosts, including bacteria, fungi, and mammals
92^{23,24}. These functional amyloid structures are capable of multiple roles in biology. For
93 example, they can provide structural support to maintain the integrity of biological structures
94²⁵, promote adhesion for organisms to surfaces or to each other²⁶, facilitate the formation of

95 protective barriers or matrices to shield cells from environmental stresses²⁴, and contribute to
96 long-term memory storage²⁷.

97

98 Recent rapid advances in amyloid structural biology methodologies have resulted in detailed
99 maps of amyloid fibril structures¹⁴. These advances have also revealed a key characteristic of
100 amyloid assembly in their capacity for displaying structural polymorphism, wherein protein
101 or peptide precursors of identical amino acid sequence can assemble into a variety of distinct
102 fibril structures, often called polymorphs. Amyloid formation, even under identical
103 environmental conditions, may result in highly complex and heterogeneous samples¹². The
104 high degree of amyloid sample heterogeneity has been observed regardless of if the fibrils
105 were formed in vitro or purified from human patients' tissues^{3,28,29}. The limited availability
106 of analysis workflows to quantify and analyse the nuanced variation between structural
107 features of amyloid polymorphs poses further challenge. This has rendered traditional
108 structural biology methods such as X-ray crystallography unable to resolve the detailed
109 structures of amyloid. Instead, advances in solid-state nuclear magnetic resonance
110 spectroscopy (ssNMR) and cryogenic transmission electron microscopy (cryo-EM) have
111 resulted in structural understanding of amyloid fibrils at near-atomic details, including
112 amyloid fibrils purified from post-mortem human brain tissues^{28,30}. In particular, the
113 'resolution revolution' of cryo-EM saw drastic improvement in the resolution of single-
114 particle 3D reconstructions of biological structures such as amyloid fibrils in the past half-
115 decade. What was previously a low to moderate resolution technique, cryo-EM is now
116 capable of providing near-atomic resolution maps of amyloid cores typically at 3Å or better
117 ^{12,31}.

118

119 While cryo-EM and ssNMR offered valuable insights into the core architecture of *in vitro*
120 assembled or *ex vivo* amyloid fibrils purified from human patient tissues, they provide static,
121 averaged snapshots of one or few highly populated polymorphs in typically highly complex
122 amyloid populations. Therefore, for polymorphous amyloid fibrils, methods that can
123 interrogate individual or rarely populated structures in addition to average structures of those
124 in the majority have become important if key questions on the polymorph structure-function
125 relationships, the environmental conditions that trigger the pathway leading to misfolding and
126 aggregation, and the influences by the conditions or minor fluctuations in the initial
127 monomeric protein structure on the speed of fibril formation and the types of abnormal
128 species formed, are to be resolved. Super-resolution microscopy (SRM) has shown potential
129 to resolve individual amyloid filaments in aqueous environments, and the resolution
130 necessary for individual filament structural characterisations can be reached through the use
131 of transiently bound fluorescent dyes and deconvolution algorithms³². Crucially, SRM is
132 capable of allowing dynamic processes such as fibril elongation to be observed on an
133 individual filament level^{32,33}. Resolving complex structures *in situ* in cells or in tissue can be
134 achieved through cryogenic electron tomography (cryo-ET)³⁴. In terms of amyloid structures,
135 cryo-ET presents an important opportunity in that it is capable of resolving individual
136 filament structures *in situ* in tissue sections, which reveal information that can potentially be
137 used for localisation and spatial correlation studies. However, similar to cryo-EM, cross-
138 particle averaging by subtomogram averaging methods must currently be carried out from the
139 low signal-to-noise ratio cryo-ET tomograms to generate averaged structural maps that are of
140 sufficiently high resolution to be used in template matching analysis to known filament
141 structures³⁵. Thus, neither SRM nor cryo-ET can resolve sufficient structural details at
142 individual filament level from a single observation to allow quantitative comparative
143 structural analysis or structural analysis of rare species. These challenges and limitations have

144 stimulated development of an AFM based individual particle level structural analysis
145 approach.

146

147 AFM is capable of a broad spectrum of imaging applications spanning from live cells to
148 individual molecules³⁶. It has also been applied to probe dynamics³⁷⁻³⁹ and molecular
149 responses to mechanical force⁴⁰ in air and liquid environments⁴¹⁻⁴³. The physics of AFM
150 relies on the interaction between the sample surface and the probe, which comprises of a
151 molecularly sharp conical tip attached to a cantilever spring. As the AFM tip scans across the
152 sample in the x/y plane, high signal-to-noise ratio z-height topography images, with sub-
153 Ångstrom noise levels, can be generated⁴⁴. AFM imaging has been previously used to
154 characterise the size distributions⁴⁵⁻⁴⁹ and the morphological features⁵⁰⁻⁵² of amyloid
155 populations by morphometric and dimensions analysis on an individual filament level.
156 Recently, the CPR-AFM method has been developed to extract the 3D information encoded
157 in the height topology images and the necessary information to reconstruct 3D surface
158 envelope models of individual helical amyloid fibrils^{3,4,15-17}.

159

160

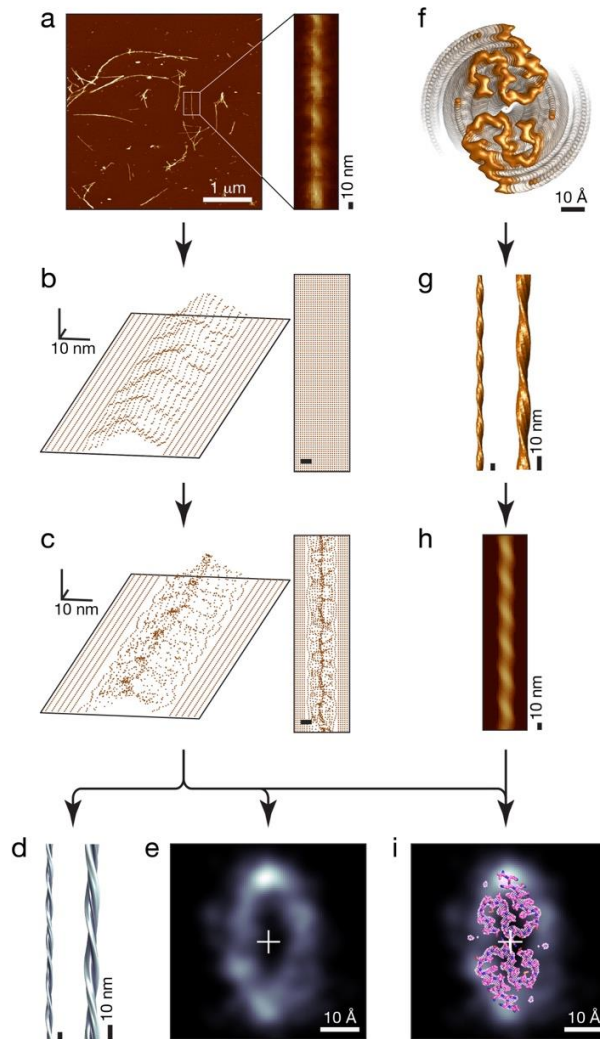
161 **CPR-AFM and 3D reconstruction of individual helical amyloid filaments**

162

163 In essence, the key conceptual idea utilised in the CPR-AFM algorithm is the realisation that
164 useful 3D information is encoded in the two-dimensional (2D) AFM height images,
165 essentially as 3D point clouds⁴ (**Figure 1**). A point cloud is a discrete set of data points in
166 space that is not gridded in the way pixels or voxels are gridded in conventional images. For
167 AFM height image data, the pixel values representing the z-coordinates are recorded when
168 the sample surface comes into contact anywhere on the probe tip. The recorded centre

169 coordinates of the tip, therefore, do not represent the actual contact points. This is commonly
170 referred to as the tip-sample convolution artefact ⁵³. The post-experiment CPR-AFM
171 algorithm estimates the 3D coordinates of the actual contact points in 3D space, effectively
172 moving the recorded tip positions off the pixel grid to subpixel locations ¹⁷. Advantageously,
173 the spatial resolution of the information encoded in the data may, therefore, be higher than
174 the estimates based on the distance between the pixels on the image grid for globular or
175 cylindrical filament structures where the actual contact points are on average more closely
176 spaced than the pixels of the original height image ¹⁷. The resulting 3D contact point cloud
177 can be subsequently used to reconstruct the 3D surface envelope of the molecular surface that
178 has interacted with the tip during imaging. In addition, for helical structures such as amyloid
179 fibrils, the 3D surface envelope of the whole filament can be reconstructed since the
180 molecular surfaces around the whole of the filament cross-sections can be inferred using tip-
181 sample contact points from a single side of the helical filament due to the helical symmetry
182 ^{4,17}.

183



184

185 **Figure 1:** Workflow summary of individual helical filaments structural analysis through 3D contact point
 186 reconstruction. a) Selection of an example individual filament segment to be analysed from an AFM height
 187 topology image. The example image of amyloid fibrils formed in vitro from human A β 42 is shown with a 1 μ m
 188 scale bar, and a 180 nm segment of the isolated individual filament is shown with scale bar indicating 10 nm. b)
 189 The helical axis is estimated for the selected fibril. The pixel z-height values of axis aligned image are shown in
 190 the 3D plot and the 2D plot shows the original pixel grid of the image. The scale bars indicate 10nm in all axes
 191 directions. c) CPR-AFM estimates the tip-sample contact points as seen in the 3D plot and moves the recorded
 192 values off the pixel grid as seen in the 2D plot. The scale bars indicate 10nm in all axes directions. d) 3D
 193 surface envelope model of the filament from a) with a 2x zoomed-in view reconstructed from the 3D contact
 194 point cloud from c). The scale bars indicate 10nm. e) Contact point density map of the filament cross-section.
 195 The scale bar indicate 10Å. f) Cryo-EM derived map of type II A β 42 amyloid fibril purified from human patients
 196 (EMD-15771⁵⁴). The scale bar indicates 10Å for the cross-sectional view. g) Helical axis aligned and extended

197 cryo-EM map constructed using f). The scale bars indicate 10 nm for the filament map and the 2x zoomed-in
198 view of the map. i) Example of an AFM height image simulated from f) and g). The simulated image can be
199 directly compared with the filament image from a). g) Molecular model (PDB: 7Q4B) or the cryo-EM derived
200 map can be fitted into the contact point density map of the filament of interest by minimising the root mean
201 square deviation (RMSD) between the 3D surface envelope and the iso-surface of cryo-EM derived map as
202 described in ¹⁶. The scale bar indicates 10Å.

203

204 In the current workflow for 3D surface envelope reconstruction of individual helical amyloid
205 filaments (see ⁴ with implementation in https://github.com/wfxue/Trace_y, **Figure 1**), a semi-
206 automatic filament tracing algorithm first isolates an individual user-selected helical filament
207 and estimates its central helical axis to sub-pixel accuracy. The tip geometry is then estimated
208 by comparing the observed filament image dilation caused by the finite size of the cantilever
209 probe tip and the expected dilation from a rounded cone tip model with a featureless
210 cylindrical approximation of the filament. The algorithm aims to find a tip radius estimate by
211 matching the calculated dilation resulting from the tip model to the observed dilation. Pre-
212 measured tip geometry parameters can also be used in this step (e.g. service provided by Nu
213 Nano Ltd, Bristol, UK for SEM analysis of AFM probes). The estimated tip-sample contact
214 points of the top of the filament in contact with the tip are then extracted as a 3D point cloud
215 using the CPR-AFM algorithm. The point cloud is subsequently aligned to the central helical
216 axis. The helical handedness of the filament twist can be established through the tilt direction
217 of the striation pattern of the filament. The helical pitch can be estimated by analysing the tilt
218 angle of the striation pattern directly in the filament image or its Fourier transformed 2D
219 power spectrum. The helical symmetry parameters are then applied to the axis-aligned
220 contact point cloud and a 3D surface envelope model of the individual filament can be
221 reconstructed using the point cloud as previously described ¹⁷. This comprehensive workflow

222 make detailed analysis of individual filaments possible even when segments as short as one
223 or two helical pitch in length is observed once in an AFM height image ¹⁷.

224

225 For the structural analysis of polymorphous amyloid fibril populations, the individual
226 filament level 3D reconstruction approach opens up several important opportunities. For
227 example, this approach offer the capacity to delve into the structural variations of complex
228 amyloid populations ¹². Individual filament level structural analysis has shown promise in the
229 quantification of sample heterogeneity, and the mapping of the polymorph distribution of
230 amyloid fibrils and its sensitivity to assembly conditions ^{3,15}. It has enabled quantitative
231 measurements of structural parameters of individual filaments such as cross-sectional radius,
232 area and shape, and twist periodicity, handedness and pitch, allowing the objective
233 discrimination of different fibril polymorphs ¹⁵. It has also allowed for the assessment of
234 structural variations within individual fibrils ¹². By integration with Cryo-EM datasets
235 available in the Electron Microscopy Data Bank (EMDB), quantitative structural analysis of
236 individual amyloid filaments formed *in vitro* from a tau sequence has identified that these
237 filaments closely resemble disease-associated paired helical filaments (PHFs) isolated from
238 brain tissues of patients ^{16,55}. More recently, individual filament level 3D reconstructions
239 were applied the *in vitro* assembly of the human 42-amino acid amyloid beta peptide (A β 42),
240 revealing the sensitivity of the fibril polymorph distribution to small changes in the assembly
241 conditions, and subtle changes in assembly conditions can exert significant influence over the
242 resulting distribution of polymorphs ³. Importantly, quantitative structural analysis on an
243 individual filament level has discovered rare species in the *in vitro* formed A β 42 amyloid
244 population that resemble amyloid polymorphs seen *ex vivo* in samples purified from human
245 patents' brains ³. These results collectively underscore the exciting potential of individual
246 particle level 3D reconstruction techniques in advancing the understanding of heterogeneous

247 polymorphous amyloid fibril populations and their biological impacts by offering insights
248 into the structural diversity, polymorphism distributions, and potential disease-associated
249 properties, as well as bridging the gap between the structures of *in vitro* and *in vivo*
250 assembled amyloid.

251

252 **Future outlook for AFM based 3D structural reconstruction**

253

254 Structural analysis of individual helical amyloid filaments by CPR-AFM offers a powerful
255 approach allowing one 3D structural reconstructions for each one individual helical filament
256 segment observed on an AFM height image, and offers a unique opportunities in addressing
257 the key questions and challenges in amyloid structural biology. One fundamental question
258 revolves around the extent of possible structural diversity of amyloid fibril populations, and
259 how the population level properties change under different *in vivo* conditions associated with
260 specific disease states^{12,14}. Structural characterisation of individual fibrils in complex and
261 heterogeneous amyloid populations⁵⁶ opens the door to the analysis and comparison of
262 population distribution and its dynamics. Understanding the connection between population-
263 level and single fibril-level properties is essential for deciphering the relationships between
264 specific polymorphs or structural properties and the phenotypic behaviours and biological
265 consequences of amyloid^{5,8,14}. Resolving filament assembly mechanisms and structural
266 polymorphism arising within individual amyloid fibrils is also a critical frontier of
267 investigations. Different polymorphs have distinct physical properties, and these differences
268 likely translate into variations in biological activities. Even when formed from identical
269 precursors and coexisting within the same population or even the same filament particle,
270 individual fibril polymorphs may exhibit varying rates of elongation, fragmentation, surface
271 activities and cytotoxic potential^{32,47}. Prions and prion-like amyloid fibrils that can propagate

272 between cells form strains that may manifest different biological activities, phenotypes and
273 localisations by its assembly ⁵⁷⁻⁶¹. AFM based individual filament level analysis may
274 rationalise the structure-function relationship between specific fibril polymorphs within a
275 heterogeneous population ‘cloud’ and their strain-specific propagation and behaviours. This
276 is of particular importance as certain fibril polymorphs may react differently to potential
277 inhibitors, leading to the development of "resistant" strains over time. Individual filament
278 level analysis may also contribute to the understanding of the time evolution of complex
279 amyloid population distributions during assembly by linking structural and quantitative
280 polymorph distribution information to the dominant intermediate structures seen by cryo-EM
281 ^{62,63}. Furthermore, understanding the factors that control the formation of dominant amyloid
282 polymorph structures, the roles of rare amyloid species, and the extent of structural variations
283 and population heterogeneity is crucial for gaining a comprehensive understanding of the
284 roles played by amyloid molecular populations in biology. Thus, population level insights
285 based on individual filament level structural analysis is essential for discerning whether some
286 amyloid aggregates act as causes or consequences of disease and how other amyloid
287 assemblies serve specific functions in physiological processes.

288

289 The 3D reconstruction approach for helical amyloid filaments has also the potential for
290 implementations in structural analysis of other types of helical structures or biological
291 structures with other symmetries. For example, the approach can be used to facilitate
292 individual filament level structural studies of helical DNA, cytoskeletal and collagen
293 filaments. Future developments may allow for the 3D reconstruction of bio-structures with
294 different symmetries, such as icosahedral viral capsids.

295

296 Structural reconstructions of individual helical filaments using 3D contact point clouds
 297 extracted from AFM height images by CPR-AFM^{4,17} unequivocally demonstrated that useful
 298 3D reconstructions of biological macromolecules are possible from AFM data. It further
 299 demonstrated for this type of soft material structures that 3D surface envelopes of
 300 intermediate spatial resolution around $\sim 10\text{\AA}$ (estimated by Fourier Ring Correlation, FRC,
 301 and the $\frac{1}{2}$ -bit information criterion)^{4,17}, a resolution range that is useful for quantitative and
 302 comparative structural analysis, and molecular identification based on template matching and
 303 model fitting approaches, can be achieved on individual particle basis where one single
 304 observation can lead to one useful 3D model. Factors based on the current limits of the
 305 fundamental physics of AFM hardware such as the probe tip radius, scanner and environment
 306 stability influence the quality of the structural data generated, and subsequently, the
 307 resolution limit of the 3D reconstruction. Synergies between CPR-AFM and three other
 308 recent developments in AFM technologies: High-Speed AFM (HS-AFM), localisation AFM
 309 (L-AFM) and simulation AFM (S-AFM) may increase the resolution of reconstructed 3D
 310 models and provide an exciting outlook for AFM as an emerging general structural biology
 311 method with the crucial individual particle 3D reconstruction capabilities (**Table 1**).

312

313 *Table 1: Summary of AFM methods that enable or could improve 3D reconstruction of individual bio-*
 314 *macromolecules.*

315

AFM method		Capability	Significance for 3D reconstruction of individual bio-macromolecules	Relevant References
AFM	(Conventional) Atomic Force Microscopy	Topological height imaging through different modes of operation, including contact, non-contact, tapping and force-distance curve-based modes.	Encodes 3D structural information of the scanned surface in topological height images.	Different AFM modes are reviewed in ² , and the widely used Gwyddion software is described in ¹⁸
HS-AFM	High-Speed AFM	Allows image data	Synergy with CPR-	Reviewed in ^{64,65} ,

		acquisition at a temporal resolution of ~100 ms	AFM could allow for increased contact point cloud dataset size, thereby improving potential spatial resolution, and for acquisition of dynamic 3D contact point clouds, thereby allowing for analyses of structural dynamics.	and example application for amyloid research in ^{38,39}
L-AFM	Localisation AFM	Generates 2D structural maps of molecular surfaces at near-atomic resolution	Synergy with CPR-AFM could improve the 3D spatial localisation of contact points thereby improved potential spatial resolution of 3D reconstructions.	Theory and NanoLocz software implementation described in ^{22,66}
S-AFM	Simulation AFM	Generates simulated AFM height images from existing experimental structural maps or predicted molecular models	Enables an integrative structural biology approach for individual bio-macromolecules by linking AFM with existing data (e.g. from cryo-EM or NMR) or structural predictions (e.g. AlphaFold2)	BioAFMviewer implementation described and reviewed in ^{20,65} , application example for amyloid research in ¹⁶
CPR-AFM	Contact Point Reconstruction AFM	Generates 3D contact point clouds from AFM height images that can be used for 3D structural reconstruction	Enables 3D reconstruction of individual bio-macromolecules' surface envelopes, (e.g. helical filaments)	Example application for amyloid structures and the Trace_y software implementation described in ^{4,17}

316

317 The development of HS-AFM throughout the 1990s and early 2000s have significantly
318 enhanced the temporal resolution capabilities of AFM ^{64,65}. With improvements such as
319 integrating short cantilevers, faster scanners, and improved feedback mechanisms, a temporal
320 resolution of sub-100ms can be reached with currently HS-AFM instruments ^{64,65}. This
321 advance has allowed directly visualisation and analyses of the dynamics of biological
322 processes. For individual particle 3D reconstructions, video frames from data acquired by
323 HS-AFM could improve CPR-AFM analysis by providing increased point cloud dataset size
324 for 3D reconstructions and provide dynamic 3D point clouds that can be used to analyse
325 time-dependent structural evolutions in the sub-second regime. The LAFM post-experimental
326 image analysis method ⁶⁶ is highly complementary to HS-AFM. Building on the localisation

327 analysis principles of SRM, the L-AFM algorithm is capable of enhancing the spatial
328 resolution of 2D images to $\sim 5\text{\AA}$ range^{22,66}. L-AFM can be used in two different ways. The
329 first approach involves creating localisation maps from multiple molecules recorded in one or
330 several HS-AFM video frames to observe the particle averaged time- or environment-
331 dependent conformational changes. This process typically requires information from 50 or
332 more observations of the same type of molecules. The second approach involves creating
333 localisation maps of the same individual molecules imaged by HS-AFM over time. For 3D
334 structural reconstructions, applying the 2D localisation step of both of the L-AFM approaches
335 in 3D on the contact point clouds extracted by CPR-AFM from data acquired by HS-AFM
336 could improve the spatial resolution of the reconstructed surface envelopes in 3D space. In
337 particular, individual particle 3D reconstructions could be carried out if the same individual
338 molecules is imaged by HS-AFM over time. S-AFM involves emulating the experimental
339 AFM scanning process and the interaction of the AFM probe tip with biomolecules of
340 interest computationally to generate simulated AFM topographic images^{16,20,65}. Simulations
341 are typically carried out by simulating rigid body interactions between the AFM tip and the
342 biomolecules of interest^{16,20}, although the biomolecules' response to the probing force may
343 also be taken into account in future developments⁶⁷. This approach enables integrative
344 structural biology methodologies that allow direct linkage between molecular models or
345 atomic/near-atomic resolution structural maps (e.g. from cryo-EM or NMR data) with
346 experimentally acquired AFM images^{3,16}, and can be used to identify structures observed on
347 AFM height images by model fitting and template matching techniques. Machine learning
348 and AI methods could also make significant contributions into bio-AFM applications, from
349 data analysis to autonomous software and hardware operation. For example, the AlphaFold 2
350 algorithm⁶⁸ has excelled in predicting the 3D structures of globular proteins and these
351 predictions could be matched to AFM data through S-AFM⁶⁵. Furthermore, S-AFM could

352 aid AFM based 3D reconstruction and molecular identification by generating synthetic
353 training datasets for neuronal network methods, using well-labelled structural data or
354 molecular models from public databases such as the Protein Data Bank (PDB)²⁰ or the
355 EMDB^{3,16}. Additionally, machine learning and AI techniques can help with quantifying
356 population heterogeneity, discerning distinct subpopulations and structural classifications
357 within heterogenous molecular populations distributions mapped through individual
358 molecular structural analysis (e.g.³), thereby shedding light on the complex relationships
359 between specific structures or polymorphs and the biological effects and consequences of
360 these structures. Hence, the integration of AI and machine learning methods could further
361 advance AFM based 3D structural analysis on individual molecular level.

362

363

364 **Conclusions**

365

366 In conclusion, an AFM based individual particle level 3D structural reconstruction method
367 has already shown its potential to address key challenges presented by polymorphous and
368 heterogeneous amyloid molecular populations and complex amyloid structure-function
369 relationships^{3,12,15,16,56}. AFM is already an indispensable tool for the analysis of a range of
370 bio-structures including DNA/RNA^{21,41,69}, membrane proteins^{37,70}, virus particles^{71,72},
371 cytoskeletal filaments^{73,74} and cell surfaces⁷⁵, in multimodal imaging modes that can also
372 incorporate optical, confocal, IR, Raman and nano-mechanical information. Future
373 developments in improving the individual particle 3D structural reconstructions capabilities
374 of CPR-AFM and in furthering its synergies with other AFM methods such as HS-AFM, L-
375 AFM and S-AFM present an exciting area of development that will undoubtedly lead to a
376 unique capability for AFM in 3D reconstruction of individual dynamic bio-macromolecule

377 structures under ambient aqueous conditions. These advances together with the broad range
378 of existing multimodal bio-AFM applications will open up exciting future opportunities for
379 AFM, forming the profile of a general, accessible, unique structural biology tool for the
380 analysis of individual bio-molecules, and taking a step closer to the structural biologists'
381 dream of being able to obtain one high detailed, dynamic and multimodal 3D structural map
382 from one single observation of one individual molecule.

383

384

385

386

387 **Perspectives**

388

389 – AFM is emerging as an indispensable tool for the structural analysis of single, individual
390 polymorphous helical amyloid filament structures through recent advances in AFM based 3D
391 structural reconstruction

392 – The key conceptual idea utilised in the 3D contact point reconstruction (CPR-AFM)
393 algorithm is the realisation that useful 3D information is encoded in the 2D AFM height
394 images as 3D point clouds.

395 – Future developments in improving the individual particle level 3D structural
396 reconstructions capabilities of CPR-AFM by furthering its synergies with other AFM
397 methods such as HS-AFM, L-AFM and S-AFM present an exciting area of development.
398 These together with machine learning, computer vision and AI analysis methods in new
399 software advances will undoubtedly lead to a unique capability for AFM in 3D reconstruction
400 of individual dynamic bio-macromolecule structures under ambient aqueous conditions.

401

402

403 **References**

404

- 405 1 Binnig, G., Quate, C. F. & Gerber, C. Atomic force microscope. *Phys Rev Lett* **56**,
406 930-933, (1986). <https://doi.org/10.1103/PhysRevLett.56.930>
- 407 2 Dumitru, A. C. & Koehler, M. Recent advances in the application of atomic force
408 microscopy to structural biology. *J Struct Biol* **215**, 107963, (2023).
409 <https://doi.org/10.1016/j.jsb.2023.107963>
- 410 3 Aubrey, L. D., Lutter, L., Fennell, K., Purton, T. J., Ward, N., Serpell, L. C. *et al.*
411 Structural reconstruction of individual filaments in Abeta42 fibril populations
412 assembled in vitro reveal rare species that resemble ex vivo amyloid polymorphs from
413 human brains. *bioRxiv*, 2023.2007.2014.549001, (2023).
414 <https://doi.org/10.1101/2023.07.14.549001>

415 4 Xue, W. F. Trace_y: Software algorithms for structural analysis of individual helical
416 filaments by three-dimensional contact point reconstruction atomic force microscopy.
417 *bioRxiv*, 547812, (2023). <https://doi.org/10.1101/2023.07.05.547812>

418 5 Ke, P. C., Zhou, R., Serpell, L. C., Riek, R., Knowles, T. P. J., Lashuel, H. A. *et al.*
419 Half a century of amyloids: past, present and future. *Chem Soc Rev* **49**, 5473-5509,
420 (2020). <https://doi.org/10.1039/c9cs00199a>

421 6 Dobson, C. M., Knowles, T. P. J. & Vendruscolo, M. The Amyloid Phenomenon and
422 Its Significance in Biology and Medicine. *Cold Spring Harb Perspect Biol* **12**, (2020).
423 <https://doi.org/10.1101/cshperspect.a033878>

424 7 Lutter, L., Serpell, C. J., Tuite, M. F. & Xue, W. F. The molecular lifecycle of
425 amyloid - Mechanism of assembly, mesoscopic organisation, polymorphism,
426 suprastructures, and biological consequences. *Biochim Biophys Acta Proteins
427 Proteom* **1867**, 140257, (2019). <https://doi.org/10.1016/j.bbapap.2019.07.010>

428 8 Chiti, F. & Dobson, C. M. Protein Misfolding, Amyloid Formation, and Human
429 Disease: A Summary of Progress Over the Last Decade. *Annu Rev Biochem* **86**, 27-68,
430 (2017). <https://doi.org/10.1146/annurev-biochem-061516-045115>

431 9 Sunde, M., Serpell, L. C., Bartlam, M., Fraser, P. E., Pepys, M. B. & Blake, C. C.
432 Common core structure of amyloid fibrils by synchrotron X-ray diffraction. *J Mol
433 Biol* **273**, 729-739, (1997). <https://doi.org/10.1006/jmbi.1997.1348>

434 10 Bonar, L., Cohen, A. S. & Skinner, M. M. Characterization of the amyloid fibril as a
435 cross-beta protein. *Proc Soc Exp Biol Med* **131**, 1373-1375, (1969).
436 <https://doi.org/10.3181/00379727-131-34110>

437 11 Eanes, E. D. & Glenner, G. G. X-ray diffraction studies on amyloid filaments. *J
438 Histochem Cytochem* **16**, 673-677, (1968). <https://doi.org/10.1177/16.11.673>

439 12 Lutter, L., Aubrey, L. D. & Xue, W. F. On the Structural Diversity and Individuality
440 of Polymorphic Amyloid Protein Assemblies. *J Mol Biol* **433**, 167124, (2021).
441 <https://doi.org/10.1016/j.jmb.2021.167124>

442 13 Close, W., Neumann, M., Schmidt, A., Hora, M., Annamalai, K., Schmidt, M. *et al.*
443 Physical basis of amyloid fibril polymorphism. *Nat Commun* **9**, 699, (2018).
444 <https://doi.org/10.1038/s41467-018-03164-5>

445 14 Scheres, S. H., Zhang, W., Falcon, B. & Goedert, M. Cryo-EM structures of tau
446 filaments. *Curr Opin Struct Biol* **64**, 17-25, (2020).
447 <https://doi.org/10.1016/j.sbi.2020.05.011>

448 15 Aubrey, L. D., Blakeman, B. J. F., Lutter, L., Serpell, C. J., Tuite, M. F., Serpell, L. C.
449 *et al.* Quantification of amyloid fibril polymorphism by nano-morphometry reveals
450 the individuality of filament assembly. *Commun Chem* **3**, 125, (2020).
451 <https://doi.org/10.1038/s42004-020-00372-3>

452 16 Lutter, L., Al-Hilaly, Y. K., Serpell, C. J., Tuite, M. F., Wischik, C. M., Serpell, L. C.
453 *et al.* Structural Identification of Individual Helical Amyloid Filaments by Integration
454 of Cryo-Electron Microscopy-Derived Maps in Comparative Morphometric Atomic
455 Force Microscopy Image Analysis. *J Mol Biol* **434**, 167466, (2022).
456 <https://doi.org/10.1016/j.jmb.2022.167466>

457 17 Lutter, L., Serpell, C. J., Tuite, M. F., Serpell, L. C. & Xue, W. F. Three-dimensional
458 reconstruction of individual helical nano-filament structures from atomic force
459 microscopy topographs. *Biomol Concepts* **11**, 102-115, (2020).
460 <https://doi.org/10.1515/bmc-2020-0009>

461 18 Nečas, David & Klapetek, Petr. Gwyddion: an open-source software for SPM data
462 analysis. *Open Physics* **10**, 181-188, (2012). [https://doi.org/doi:10.2478/s11534-011-](https://doi.org/doi:10.2478/s11534-011-0096-2)
463 [0096-2](https://doi.org/doi:10.2478/s11534-011-0096-2)

- 464 19 Usov, I. & Mezzenga, R. FiberApp: An Open-Source Software for Tracking and
465 Analyzing Polymers, Filaments, Biomacromolecules, and Fibrous Objects.
466 *Macromolecules* **48**, 1269-1280, (2015). <https://doi.org/10.1021/ma502264c>
- 467 20 Amyot, R. & Flechsig, H. BioAFMviewer: An interactive interface for simulated
468 AFM scanning of biomolecular structures and dynamics. *PLoS Comput Biol* **16**,
469 e1008444, (2020). <https://doi.org/10.1371/journal.pcbi.1008444>
- 470 21 Beton, J. G., Moorehead, R., Helfmann, L., Gray, R., Hoogenboom, B. W., Joseph, A.
471 P. *et al.* TopoStats - A program for automated tracing of biomolecules from AFM
472 images. *Methods* **193**, 68-79, (2021). <https://doi.org/10.1016/j.ymeth.2021.01.008>
- 473 22 Heath, G. R., Micklethwaite, E. & Storer, T. NanoLocz: Image analysis platform for
474 AFM, high-speed AFM and localization AFM. *bioRxiv*, 2023.2011.2023.568405,
475 (2023). <https://doi.org/10.1101/2023.11.23.568405>
- 476 23 Fowler, D. M., Koulov, A. V., Balch, W. E. & Kelly, J. W. Functional amyloid--from
477 bacteria to humans. *Trends Biochem Sci* **32**, 217-224, (2007).
478 <https://doi.org/10.1016/j.tibs.2007.03.003>
- 479 24 Sonderby, T. V., Najarzadeh, Z. & Otzen, D. E. Functional Bacterial Amyloids:
480 Understanding Fibrillation, Regulating Biofilm Fibril Formation and Organizing
481 Surface Assemblies. *Molecules* **27**, (2022).
482 <https://doi.org/10.3390/molecules27134080>
- 483 25 Hobley, L., Harkins, C., MacPhee, C. E. & Stanley-Wall, N. R. Giving structure to
484 the biofilm matrix: an overview of individual strategies and emerging common
485 themes. *FEMS Microbiol Rev* **39**, 649-669, (2015).
486 <https://doi.org/10.1093/femsre/fuv015>
- 487 26 Chapman, M. R., Robinson, L. S., Pinkner, J. S., Roth, R., Heuser, J., Hammar, M. *et*
488 *al.* Role of Escherichia coli curli operons in directing amyloid fiber formation.
489 *Science* **295**, 851-855, (2002). <https://doi.org/10.1126/science.1067484>
- 490 27 Hervas, R., Rau, M. J., Park, Y., Zhang, W., Murzin, A. G., Fitzpatrick, J. A. J. *et al.*
491 Cryo-EM structure of a neuronal functional amyloid implicated in memory
492 persistence in Drosophila. *Science* **367**, 1230-1234, (2020).
493 <https://doi.org/10.1126/science.aba3526>
- 494 28 Yang, Y., Arseni, D., Zhang, W., Huang, M., Lovestam, S., Schweighauser, M. *et al.*
495 Cryo-EM structures of amyloid-beta 42 filaments from human brains. *Science* **375**,
496 167-172, (2022). <https://doi.org/10.1126/science.abm7285>
- 497 29 Meinhardt, J., Sachse, C., Hortschansky, P., Grigorieff, N. & Fandrich, M. Abeta(1-
498 40) fibril polymorphism implies diverse interaction patterns in amyloid fibrils. *J Mol*
499 *Biol* **386**, 869-877, (2009). <https://doi.org/10.1016/j.jmb.2008.11.005>
- 500 30 Fitzpatrick, A. W. P., Falcon, B., He, S., Murzin, A. G., Murshudov, G., Garringer, H.
501 J. *et al.* Cryo-EM structures of tau filaments from Alzheimer's disease. *Nature* **547**,
502 185-190, (2017). <https://doi.org/10.1038/nature23002>
- 503 31 Louros, N., van der Kant, R., Schymkowitz, J. & Rousseau, F. StAmP-DB: a platform
504 for structures of polymorphic amyloid fibril cores. *Bioinformatics* **38**, 2636-2638,
505 (2022). <https://doi.org/10.1093/bioinformatics/btac126>
- 506 32 Sun, Y., Jack, K., Ercolani, T., Sangar, D., Hosszu, L., Collinge, J. *et al.* Direct
507 Observation of Competing Prion Protein Fibril Populations with Distinct Structures
508 and Kinetics. *ACS Nano* **17**, 6575-6588, (2023).
509 <https://doi.org/10.1021/acsnano.2c12009>
- 510 33 Young, L. J., Kaminski Schierle, G. S. & Kaminski, C. F. Imaging Abeta(1-42) fibril
511 elongation reveals strongly polarised growth and growth incompetent states. *Phys*
512 *Chem Chem Phys* **19**, 27987-27996, (2017). <https://doi.org/10.1039/c7cp03412a>

- 513 34 Lucic, V., Rigort, A. & Baumeister, W. Cryo-electron tomography: the challenge of
514 doing structural biology in situ. *J Cell Biol* **202**, 407-419, (2013).
515 <https://doi.org/10.1083/jcb.201304193>
- 516 35 Gilbert, M. A. G., Fatima, N., Jenkins, J., O'Sullivan, T. J., Schertel, A., Halfon, Y. *et al.*
517 In situ cryo-electron tomography of β -amyloid and tau in post-mortem
518 Alzheimer's disease brain. *bioRxiv*, 2023.2007.2017.549278, (2023).
519 <https://doi.org/10.1101/2023.07.17.549278>
- 520 36 Dufrene, Y. F., Ando, T., Garcia, R., Alsteens, D., Martinez-Martin, D., Engel, A. *et al.*
521 Imaging modes of atomic force microscopy for application in molecular and cell
522 biology. *Nat Nanotechnol* **12**, 295-307, (2017). <https://doi.org/10.1038/nnano.2017.45>
- 523 37 Parsons, E. S., Stanley, G. J., Pyne, A. L. B., Hodel, A. W., Nievergelt, A. P., Menny,
524 A. *et al.* Single-molecule kinetics of pore assembly by the membrane attack complex.
525 *Nat Commun* **10**, 2066, (2019). <https://doi.org/10.1038/s41467-019-10058-7>
- 526 38 Watanabe-Nakayama, T., Ono, K., Itami, M., Takahashi, R., Teplow, D. B. &
527 Yamada, M. High-speed atomic force microscopy reveals structural dynamics of
528 amyloid beta1-42 aggregates. *Proc Natl Acad Sci U S A* **113**, 5835-5840, (2016).
529 <https://doi.org/10.1073/pnas.1524807113>
- 530 39 Konno, H., Watanabe-Nakayama, T., Uchihashi, T., Okuda, M., Zhu, L., Kodera, N.
531 *et al.* Dynamics of oligomer and amyloid fibril formation by yeast prion Sup35
532 observed by high-speed atomic force microscopy. *Proc Natl Acad Sci U S A* **117**,
533 7831-7836, (2020). <https://doi.org/10.1073/pnas.1916452117>
- 534 40 Chen, Y., Radford, S. E. & Brockwell, D. J. Force-induced remodelling of proteins
535 and their complexes. *Curr Opin Struct Biol* **30**, 89-99, (2015).
536 <https://doi.org/10.1016/j.sbi.2015.02.001>
- 537 41 Ares, P., Fuentes-Perez, M. E., Herrero-Galan, E., Valpuesta, J. M., Gil, A., Gomez-
538 Herrero, J. *et al.* High resolution atomic force microscopy of double-stranded RNA.
539 *Nanoscale* **8**, 11818-11826, (2016). <https://doi.org/10.1039/c5nr07445b>
- 540 42 Nowakowski, R., Luckham, P. & Winlove, P. Imaging erythrocytes under
541 physiological conditions by atomic force microscopy. *Biochim Biophys Acta* **1514**,
542 170-176, (2001). [https://doi.org/10.1016/s0005-2736\(01\)00365-0](https://doi.org/10.1016/s0005-2736(01)00365-0)
- 543 43 Moreno-Herrero, F., Perez, M., Baro, A. M. & Avila, J. Characterization by atomic
544 force microscopy of Alzheimer paired helical filaments under physiological
545 conditions. *Biophys J* **86**, 517-525, (2004). [https://doi.org/10.1016/S0006-3495\(04\)74130-2](https://doi.org/10.1016/S0006-3495(04)74130-2)
- 546
- 547 44 Alessandrini, A. & Facci, P. AFM: a versatile tool in biophysics. *Meas Sci Technol* **16**,
548 R65-R92, (2005). <https://doi.org/10.1088/0957-0233/16/6/R01>
- 549 45 Beal, D. M., Tournus, M., Marchante, R., Purton, T. J., Smith, D. P., Tuite, M. F. *et al.*
550 The Division of Amyloid Fibrils: Systematic Comparison of Fibril Fragmentation
551 Stability by Linking Theory with Experiments. *iScience* **23**, 101512, (2020).
552 <https://doi.org/10.1016/j.isci.2020.101512>
- 553 46 Marchante, R., Beal, D. M., Koloteva-Levine, N., Purton, T. J., Tuite, M. F. & Xue,
554 W. F. The physical dimensions of amyloid aggregates control their infective potential
555 as prion particles. *Elife* **6**, e27109, (2017). <https://doi.org/10.7554/eLife.27109>
- 556 47 Sanami, S., Purton, T. J., Smith, D. P., Tuite, M. F. & Xue, W. F. Comparative
557 Analysis of the Relative Fragmentation Stabilities of Polymorphic Alpha-Synuclein
558 Amyloid Fibrils. *Biomolecules* **12**, 630, (2022).
559 <https://doi.org/10.3390/biom12050630>
- 560 48 Xue, W. F., Hellewell, A. L., Gosal, W. S., Homans, S. W., Hewitt, E. W. & Radford,
561 S. E. Fibril fragmentation enhances amyloid cytotoxicity. *J Biol Chem* **284**, 34272-
562 34282, (2009). <https://doi.org/10.1074/jbc.M109.049809>

563 49 Xue, W. F. & Radford, S. E. An imaging and systems modeling approach to fibril
564 breakage enables prediction of amyloid behavior. *Biophys J* **105**, 2811-2819, (2013).
565 <https://doi.org/10.1016/j.bpj.2013.10.034>

566 50 Adamcik, J. & Mezzenga, R. Amyloid Polymorphism in the Protein Folding and
567 Aggregation Energy Landscape. *Angew Chem Int Ed Engl* **57**, 8370-8382, (2018).
568 <https://doi.org/10.1002/anie.201713416>

569 51 Ruggeri, F. S., Flagmeier, P., Kumita, J. R., Meisl, G., Chirgadze, D. Y., Bongiovanni,
570 M. N. *et al.* The Influence of Pathogenic Mutations in alpha-Synuclein on Biophysical
571 and Structural Characteristics of Amyloid Fibrils. *ACS Nano* **14**, 5213-5222, (2020).
572 <https://doi.org/10.1021/acsnano.9b09676>

573 52 Koloteva-Levine, N., Aubrey, L. D., Marchante, R., Purton, T. J., Hiscock, J. R.,
574 Tuite, M. F. *et al.* Amyloid particles facilitate surface-catalyzed cross-seeding by
575 acting as promiscuous nanoparticles. *Proc Natl Acad Sci U S A* **118**, e2104148118,
576 (2021). <https://doi.org/10.1073/pnas.2104148118>

577 53 Villarrubia, J. S. Algorithms for Scanned Probe Microscope Image Simulation,
578 Surface Reconstruction, and Tip Estimation. *J Res Natl Inst Stand Technol* **102**, 425-
579 454, (1997). <https://doi.org/10.6028/jres.102.030>

580 54 Stern, A. M., Yang, Y., Jin, S., Yamashita, K., Meunier, A. L., Liu, W. *et al.*
581 Abundant Abeta fibrils in ultracentrifugal supernatants of aqueous extracts from
582 Alzheimer's disease brains. *Neuron* **111**, 2012-2020 e2014, (2023).
583 <https://doi.org/10.1016/j.neuron.2023.04.007>

584 55 Al-Hilaly, Y. K., Marshall, K. E., Lutter, L., Biasseti, L., Mengham, K., Harrington, C.
585 R. *et al.* An Additive-Free Model for Tau Self-Assembly. *Methods Mol Biol* **2551**,
586 163-188, (2023). https://doi.org/10.1007/978-1-0716-2597-2_12

587 56 Konstantoulea, K., Guerreiro, P., Ramakers, M., Louros, N., Aubrey, L. D., Houben,
588 B. *et al.* Heterotypic Amyloid beta interactions facilitate amyloid assembly and
589 modify amyloid structure. *EMBO J* **41**, e108591, (2022).
590 <https://doi.org/10.15252/emboj.2021108591>

591 57 Kaufman, S. K., Sanders, D. W., Thomas, T. L., Ruchinkas, A. J., Vaquer-Alicea, J.,
592 Sharma, A. M. *et al.* Tau Prion Strains Dictate Patterns of Cell Pathology, Progression
593 Rate, and Regional Vulnerability In Vivo. *Neuron* **92**, 796-812, (2016).
594 <https://doi.org/10.1016/j.neuron.2016.09.055>

595 58 Collinge, J. & Clarke, A. R. A general model of prion strains and their pathogenicity.
596 *Science* **318**, 930-936, (2007). <https://doi.org/10.1126/science.1138718>

597 59 Bateman, D. A. & Wickner, R. B. The [PSI⁺] prion exists as a dynamic cloud of
598 variants. *PLoS Genet* **9**, e1003257, (2013).
599 <https://doi.org/10.1371/journal.pgen.1003257>

600 60 Jucker, M. & Walker, L. C. Self-propagation of pathogenic protein aggregates in
601 neurodegenerative diseases. *Nature* **501**, 45-51, (2013).
602 <https://doi.org/10.1038/nature12481>

603 61 Kundel, F., Hong, L., Falcon, B., McEwan, W. A., Michaels, T. C. T., Meisl, G. *et al.*
604 Measurement of Tau Filament Fragmentation Provides Insights into Prion-like
605 Spreading. *ACS Chem Neurosci* **9**, 1276-1282, (2018).
606 <https://doi.org/10.1021/acchemneuro.8b00094>

607 62 Lovestam, S., Li, D., Wagstaff, J. L., Kotecha, A., Kimanius, D., McLaughlin, S. H.
608 *et al.* Disease-specific tau filaments assemble via polymorphic intermediates. *Nature*
609 **625**, 119-125, (2024). <https://doi.org/10.1038/s41586-023-06788-w>

610 63 Wilkinson, M., Xu, Y., Thacker, D., Taylor, A. I. P., Fisher, D. G., Gallardo, R. U. *et*
611 *al.* Structural evolution of fibril polymorphs during amyloid assembly. *Cell* **186**,
612 5798-5811 e5726, (2023). <https://doi.org/10.1016/j.cell.2023.11.025>

613 64 Ando, T., Uchihashi, T. & Kodera, N. High-speed AFM and applications to
614 biomolecular systems. *Annu Rev Biophys* **42**, 393-414, (2013).
615 <https://doi.org/10.1146/annurev-biophys-083012-130324>
616 65 Flechsig, H. & Ando, T. Protein dynamics by the combination of high-speed AFM
617 and computational modeling. *Curr Opin Struct Biol* **80**, 102591, (2023).
618 <https://doi.org/10.1016/j.sbi.2023.102591>
619 66 Heath, G. R., Kots, E., Robertson, J. L., Lansky, S., Khelashvili, G., Weinstein, H. *et al.*
620 Localization atomic force microscopy. *Nature* **594**, 385-390, (2021).
621 <https://doi.org/10.1038/s41586-021-03551-x>
622 67 Sumikama, T. Computation of topographic and three-dimensional atomic force
623 microscopy images of biopolymers by calculating forces. *Biophys Rev-Ger*, (2023).
624 <https://doi.org/10.1007/s12551-023-01167-1>
625 68 Jumper, J., Evans, R., Pritzel, A., Green, T., Figurnov, M., Ronneberger, O. *et al.*
626 Highly accurate protein structure prediction with AlphaFold. *Nature* **596**, 583-589,
627 (2021). <https://doi.org/10.1038/s41586-021-03819-2>
628 69 Pyne, A., Thompson, R., Leung, C., Roy, D. & Hoogenboom, B. W. Single-molecule
629 reconstruction of oligonucleotide secondary structure by atomic force microscopy.
630 *Small* **10**, 3257-3261, (2014). <https://doi.org/10.1002/sml.201400265>
631 70 Whited, A. M. & Park, P. S. Atomic force microscopy: a multifaceted tool to study
632 membrane proteins and their interactions with ligands. *Biochim Biophys Acta* **1838**,
633 56-68, (2014). <https://doi.org/10.1016/j.bbamem.2013.04.011>
634 71 Kiss, B., Kis, Z., Palyi, B. & Kellermayer, M. S. Z. Topography, Spike Dynamics,
635 and Nanomechanics of Individual Native SARS-CoV-2 Virions. *Nano Lett* **21**, 2675-
636 2680, (2021). <https://doi.org/10.1021/acs.nanolett.0c04465>
637 72 Baclayon, M., Wuite, G. J. L. & Roos, W. H. Imaging and manipulation of single
638 viruses by atomic force microscopy. *Soft Matter* **6**, 5273-5285, (2010).
639 <https://doi.org/10.1039/b923992h>
640 73 Penedo, M., Miyazawa, K., Okano, N., Furusho, H., Ichikawa, T., Alam, M. S. *et al.*
641 Visualizing intracellular nanostructures of living cells by nanoendoscopy-AFM. *Sci*
642 *Adv* **7**, eabj4990, (2021). <https://doi.org/10.1126/sciadv.abj4990>
643 74 Kodera, N., Yamamoto, D., Ishikawa, R. & Ando, T. Video imaging of walking
644 myosin V by high-speed atomic force microscopy. *Nature* **468**, 72-76, (2010).
645 <https://doi.org/10.1038/nature09450>
646 75 Pasquina-Lemonche, L., Burns, J., Turner, R. D., Kumar, S., Tank, R., Mullin, N. *et al.*
647 The architecture of the Gram-positive bacterial cell wall. *Nature* **582**, 294-297,
648 (2020). <https://doi.org/10.1038/s41586-020-2236-6>
649